https://doi.org/10.24297/jap.v17i.8667

Preparation, characterization and antibacterial activity of pomegranate peel extract and chitosan-silver nanoparticles using electrochemical method.

A. Sarhan[a*], M. I. Abdel Hamid[a]. Sabrien A. Omar[b] and R. Hanie[a].

aPolymer Research Group, Physics Department, Faculty of Science, Mansoura University, Mansoura 35516, Egypt

b Microbiology Department, Faculty of Agriculture, Mansoura University, Mansoura 35516, Egypt

* Afaf_Sarhan2003@Yahoo.Com

Abstract

The present work involves the development of chitosan-pomegranate peel extract and silver nanoparticles (Cs-PPE-AgNPs) using electrochemical process followed by UV irradiation reduction. Formation of silver nanoparticles was characterized by by UV–vis spectroscopy, Fourier transform infrared spectroscopy (FTIR), X-ray diffraction (XRD), differential thermal analysis (DTA), scanning electron microscopy (SEM), Swelling and thermal gravimetric analysis (TGA). The obtain nanoparticles average size was 34.6 nm. UV Spectroscopy show new peak at 405 nm indicate the formation of AgNPs particles. Cs-PPE and Cs-PPE-AgNPs also demon started a relativity high antibacterial against Escherichia coli and Staphylococcus aureus bacteria.

Keywords: Chitosan; Pomegranate peel extract; Silver nanoparticles; Antibacterial activity; Electrochemical method.

1. Introduction

Chitosan is a linear polysaccharide consists of β-(1→4)-2-acetamido-D-glucose and β-(1→4)-2-amino-D-glucose units obtain by alkaline deacetylation of chitin. Chitosan has three type of function group's free amino acid, hydroxyl andacetamide group, which influence the solubility of the polymer. Chitosan has proven to be non-toxic, biodegradable, biocompatible and has an antimicrobial characteristic, so it has variety application in the medicalfields such as antitumor, wound healing and hypercholesterolemia treatment (Bui et al., 2017; Morsi et al., 2019; Zhang et al., 2010).

All parts of the pomegranate fruit (peel and seeds) consider as waste products can be processed for value-added products having industrial, medicinal, and cosmetic value. Pomegranate wastes are produced in all the phases of fruits life cycle, i.e., during agricultural production, industrial manufacturing, and processing. It is possible to take advantage of pomegranate by-products as they are a rich source of bioactive compounds such as flavonoids, phenolic acids, and tannins. Moreover, many researchers have described that pomegranate extracts, made from by-products of the processing factories, have an effective free radical scavenging activity and antioxidant capacity (Akhtar et al., 2015; Qin et al., 2015).

Furthermore, the pomegranate extracts act as natural inhibitors of pathogens, bacteria, and fungi. Pomegranate ellagitannins are hydrolyzed by gut microbiota to smaller phenolics, such as ellagic acid. Ellagic acid is then absorbed into the blood circulation, while ellagitannins are not absorbed and are metabolized into urolithins (López-Mata et al., 2013; Suntres et al., 2015).

A significant body of analysis has targeted recently on the event and characterization of nanoparticles supported noble metals (Ag, Au, Pt and Pd) owing to their uncommon characteristics compared to bulk metals additionally to their potential applications in varied fields together with magnetic, optical, catalytic, electrical, and sensing technologies (Goldsmith et al., 2014). Silver nanoparticles are one of the most universal antibacterial substances, which low concentration of it gives high antibacterial activity (De Leonardis

et al., 2008). Applications have been found for silver nanoparticles in wide range fields from electronic, antimicrobial to diagnostics and therapeutics (Fares et al., 2011). The inexperienced synthesis technique (electrochemical method) delineate within the gift study does not solely represents a cheap and comparatively fast technique for developing Cs-PPE-AgNPs however, it is additionally provide varied benefits of biocompatibility and and eco-friendliness for varied medicine and pharmaceutical applications as all the materials utilized in the study square measure renewable and environmentally benign. The objectives of the present study are to develop a composite film of (Cs-PPE) and (Cs-PPE-AgNPs) and investigate characterization, antibacterial and thermal difference between them. The main aim of this study focus in the study the change of antibacterial activity against Escherichia coli and Staphylococcus aureus happen due to adding silver nanoparticles by the electrochemical method to chitosan-pomegranate peel extract.

2. Experimental

2.1 Materials

Chitosan with a degree of deacetylation of 93% is purchase from Oxford laboratory reagent (Thani, India), Tween, glycerol, ethanol and acetic acid (EL-Naserpharamatical chemical Egypt Co. Silver plate (20 × 40 × 5) mm of purity 99.99%, are purchase from Sigma-Aldrich (St Louis, USA). The silver plate is use as the anode in the cell, polished by victimization fine abrasive, clean by dimethyl ketone, ethyl alcohol (90 %) and de-ionized water. Platinum sheet (20 × 40 × 2) mm obtain from Sigma, were use as the cathode. De-ionized water (resistivity >2x10^{8}Ω cm) was used for all samples preparation.

2.2 Method

2.2.1 Preparation of pomegranate peel extract

The dried pomegranate peel powder using a mixer grinder and 200g portions of finely pomegranate peel was blended with 80% ethanol for 2 h at 60 °C then use Ultrasonic bath for 10ml. The extracts were through filter paper (Waterman No. 1) and dried overnight in an oven at 50 °C to form crude which was stored at 4 °C until further analysis.

2.2.2 Preparation of chitosan and olive leave extract film

Chitosan solution prepared with 1% (w/w) chitosan in 1% (w/w) acetic acid at room temperature. After overnight stirring, the solution filters to remove any insoluble particles. Afterward, glycerol (glycerol/chitosan = 0.5, w/w) and Tween 80 at 0.5% (w/w) were mixed into the solution, with 30 min of stirring. Then, olive leaves extract was added to the chitosan solution (10g/l) with stirring overnight and use centrifuge (1500 rps) to remove any insoluble particles. The solution poured into glass Petri dishes and put in the oven at 50^{o}C for 24h.

2.2.3 Preparation of chitosan-pomegranate peel extract and silver nanoparticles

Cs-PPE-AgNPs is obtained using electrochemical oxidation /complexation method by using a constant potential of 1.4 V for 2h. The cell consists of 5 cm-separated silver (anode) and platinum (cathode) plates. The two electrodes were immersed vertically with in the electrolytic solution (Cs-OLE) through platinum wires that sealed to a glass tube followed by UV Irradiation reduction (λ_{max} = 254 nm at 30^{o}C for 1h) (Goldsmith et al., 2015).

2.3 Instrumentation

The UV-Vis spectra of the Cs, Cs-PPE and Cs-PPE-AgNPs recorded in the range of 200-600 nm using ATI Unicom UV-Vis. Spectrophotometer. The analysis completed at room temperature (T=303 K) with quartz

cuvettes (1 cm optical path) and the blank is 100ml water and 1 ml acetic acid. The FTIR spectra of the Cs, PPE, Cs-PPE and Cs-PPE-AgNPs were recorded in the range of 400–4000 cm^{-1}using a Mattson 5000 FTIR spectrometerat 303 Kwith resolution of 8 cm^{-1}. All sample place in the sample holder of the spectrometer. The X-ray diffraction patterns of theCs, Cs-PPE and Cs-PPE-AgNPs samples obtain utilize Philips PW 1390 X-ray diffractometer. The X-ray diffraction provides with a beam monochromatic and CuKα radiation at λ =1.5406A°. The applied voltage was 40 KV and the current intensity was 40 mA. Sec. The 2θ angle was scanned in the range of 4° to 70°, and the X-ray runs were applied at a scanning speed of 2θ=2°/min. DSC analysis carries out using a NETZSCH STA 409C/CD instrument,samples place into an aluminum pan then scale with a crimped lid and heat from 20°C to 800°C at a rate of 10°C/min with Him as carrier gas at a flow rate (50 ml/min). It was operated in the metallurgical institute (El-Tebbeen Helwan). Thermo gravimetric analyses carried out with a heating rate of 10°C/min.

2.4. Swelling studies

The ensuing Cs-PPE and Cs-PPE-AgNPs complexes method caste in 10 cm Petri dishes and dry at temperature followed by drying at 50°C for 1days. Film samples (3x4 cm) were then cut from the pure metal, Cs-PPE and Cs-PPE-AgNPs films. The thickness of the films wasexisted within the vary of 250-300 µm employing micrometer. The swelling behavior was studied by sinking the weighted samples in de-ionized water at temperature for planned intervals. The weighted samples were set as operate of your time once drying it exploitation paper to get rid of water drops. The swelling of the samples was expressed because the siharevainglorous (S%) as shown in the next equation.

$$S\% = [(W_s - W_d)/W_d] \times 100$$

Where W_d is the weight of the dry sample (g) and W_s is the weight of the swelled sample at time t.

2.5 Antibacterial assay

2.5.1 Clinical isolates

Two identified clinical isolates particularly coccus aureus (S. aureus) and Escherichia coli (E. coli) provide from biological science department, faculty of Agriculture, Mansoura University, Mansoura, Egypt. All microorganism clinical isolates maintain habitually on culture medium slants (Oxoid) at 4°C.

2.5.2 Preparation of bacterial inoculum

Twenty-fourhour nutrient broth cultures of take a look at microorganism to grow in associate orbital shaking brooder, centrifuge, wash doubly with PBS and so standardize to about 10^6 CFU ml victimisation broth meduim.

2.5.3 Bacterial sensitivity test

Standard well agar diffusion methodology carries bent on find the activity of Cs-PPE and Cs-PPE-AgNPs against the clinical microorganism isolates in step with Cheesbrough (2000) (Qin et al., 2015). For antibacterial drug activities of the compounds, wells build in plates contain culture medium seed with one hundred µl of twenty-four h of every clinical isolate. The plates were left in icebox for two h then, incubated at 37° C for twenty-four h. The diameter of inhibition zones was measured and tabulated.

2.6. Thermal stimulated depolarized current (TSDC) technique.

TSDC technique apparature consists of three main part:

First part contain cell, heater, temperature controller, thermocouple and variac to control the volt which are series connected to each other as responsible for heating the sample at constant rate.

Second part is DC power supply, which is parallel connected to sample during polarization process.

Last part is electrometer, which is parrel connected to sample and used to measure current during polarization.

3. Result and Discussion

3.1. Fourier Transform infrared Spectroscopy (FTIR).

Fourier-transform infrared (FTIR) spectroscopy use to confirm the crosslinking reaction between Cs-PPE and Cs-PPE-AgNPs. Fig. 1(a) shows FTIR spectra of chitosan(Cs) which show abroad peak at 3445 cm^{-1} which is attribute to O-H (hydroxyl group) and NH_2 (amine group), sharp peaks at (2923-2854) cm^{-1} which correspond to symmetric and asymmetric C-H and peaks appear at (1656, 1550, 1422, 1252 and 1034) cm^{-1} refer to C=O, N-H bending (amidell), aromatic ring, C-O-H and C-O stretching (Romainor et al., 2014; Silverstein & Bassler, 1962). For pomegranate extract the broad band at 3425 cm^{-1} attributed to O-H (hydroxyl group) , sharp peak at 2927 cm^{-1} corresponding to C-H stretching band and the peaks appear at 1729 ,16418, 1351 ,1228 and 1055 cm^{-1}refer to C=O of, lactones, ketones or carboxylic anhydrides, C-O stretching vibration in quinine ,C=C aromatic ring, C-O group stretching in ester, ether or phenol group and C-N stretching of aliphatic primary amine (Romainor et al., 2014). The main difference between chitosan and chitosan with pomegranate is that little shift of 2854, 1550 and 1422 cm^{-1} and decrease in strength of some peaks which indicate that there's an interaction happen (Silverstein & Bassler, 1962). For Cs-PPE-AgNPs there's shift and decrease in the strength of peak appear at 1656 and 1560 cm^{-1} happen due to binding of Ag nanoparticle with N-H and finally decrease of the peak at 1411, 1155 and 655 cm^{-1} may be happen due to increase in Ag^{+} ion observation so there's good interaction between polymer and silver nanoparticle (Ismail et al., 2014; Qi et al., 2004).

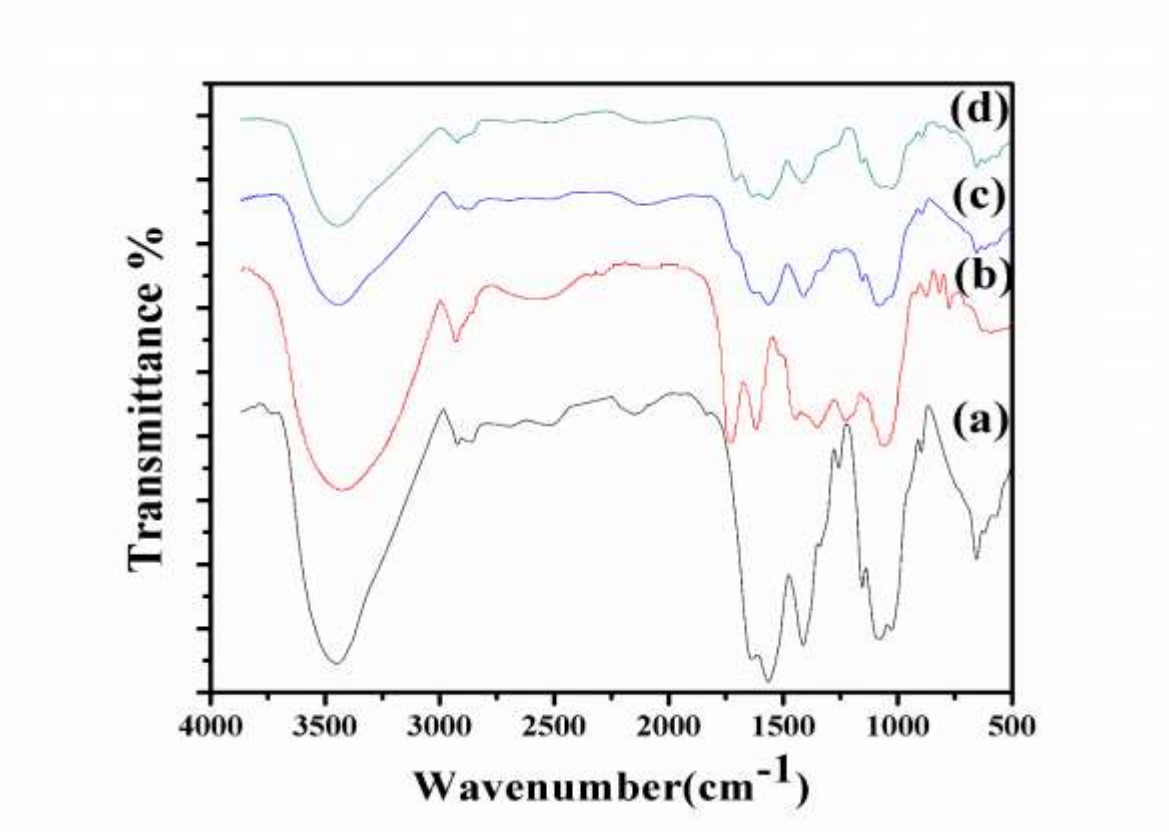

Figure 1 Show FTIR of (a) Cs, (b) PPE, (c) Cs-PPE and (d) Cs-PPE-AgNPs.

3.2 UV Spectroscopy.

UV spectroscopy for Cs shows two peaks at 213 and 243 nm which happen occur attributed to π-system of benzene ring (Liu et al., 2013). By adding PPE to Cs peak at 243nm shift to 259 nm and other peaks appear at 285, 312, 357 nm refer to PPE. In Fig. 2 λ_{max} shift from 243 to 312 then to 350 nm so, energy gap decrease from 5.10 to 3.97 then to 3.54 eV, so chitosan and pomegranate peel extract (Cs-PPE) have lower energy difference, more conjugated system and more stable than chitosan (Cs) and chitosan, pomegranate peel extract and silver nanoparticle (Cs-PPE-AgNPs) more stable than chitosan and pomegranate peel extract. All of this indicates presence of good interaction between chitosan and extract. In Fig. 2(c) by using electrochemical method to add AgNPs to Cs-PPE solution, there's a new peak appear at 405 nm refer to silver Nano particle in solution which called plasmonic resonance in UV absorption.

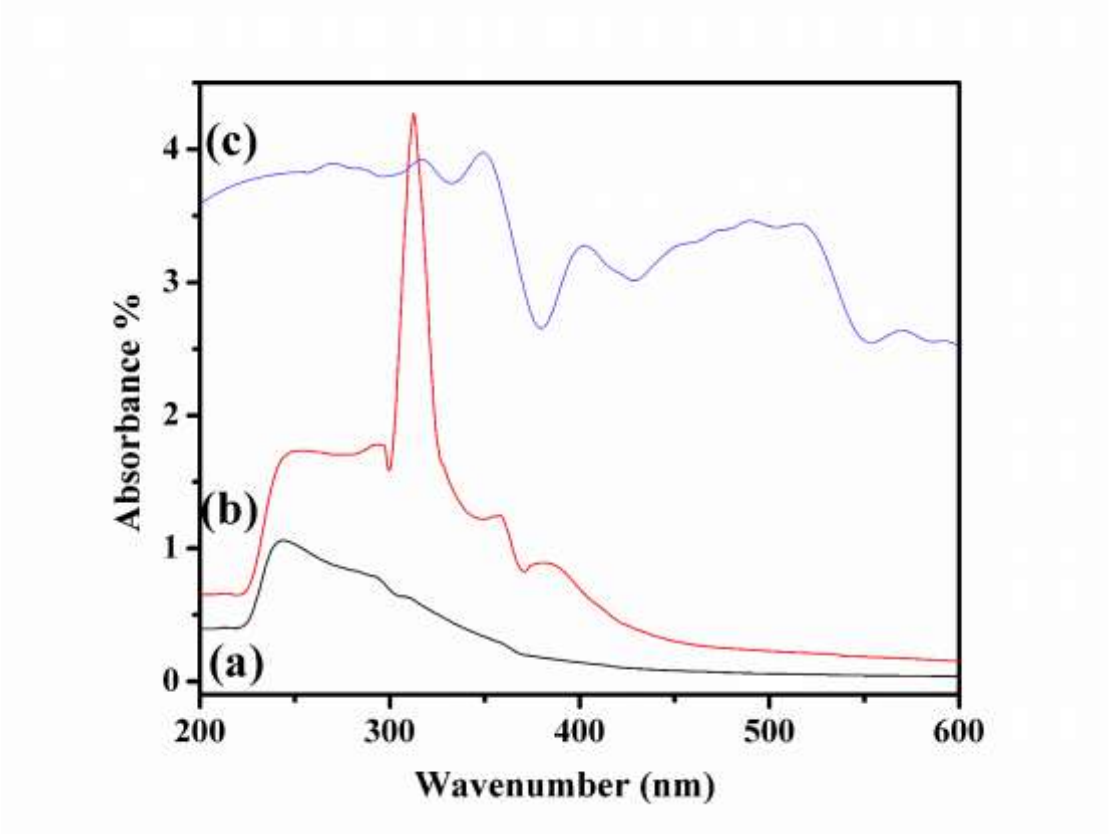

Figure 2 shows UV spectroscopy for (a) Cs, (b) Cs-PPE and (c) Cs-PPE-AgNPs.

As show in Table 1 energy gap can be calculated by this equation

$$E = \frac{hc}{\lambda}$$

Where, Energy (E) = Band gap, Planks constant (h) = 6.626×10^{-34} Joules sec, Velocity of Light (c) = 2.99×10^{8} meter/sec and Wavelength λ) = Absorption peak value. Also 1eV = 1.6×10^{-19} Joules (Conversion factor). By this formula band gap can be calculated easily, from UV-Vis spectroscopy absorption peak.

Table 1 UV maximum peak for Cs, Cs-PPE and Cs-PPE-AgNPs.

Sample	**Max wave length (nm)**	**Energy gap (eV)**
Cs	243	5.10
Cs-PPE	320	3.97
Cs-PPE-AgNPs	345	3.54

3.3. X-ray diffraction (XRD)

XRD in Fig. 3(a) shows chitosan have four peaks weak at 2θ° of 8.08°, 11.47°, 18.17° and 22.53° with degree of crystallinity equal 26.21% this degree increase for chitosan and pomegranate peel extract to 26.6% and increase again by using electrochemical method to add silver nanoparticle to 32.82% (Acosta et al., 2015). On the other hand, compare the diffractogram of Cs-PPE and Cs show that various peaks in Cs disappear in Cs-PPE diffractogram. Using electrochemical method to add AgNPs to Cs-PPE solution sharp peaks appear at 27.78, 32.22, 46.27, 54.77, 57.43, and 76.74 and which indicate presence of silver nanoparticles (Loo et al., 2012). In additions these peaks may be contribute to (111), (200), (220), (311), (222) and (311) crystallographic planes. By using the Scherrer formula $D = n\lambda/\beta\cos\theta$, where D is the crystallite size, n is a constant (=0.9 assuming that the particles are spherical), λ is the wavelength of the X-ray radiation, β is the line width (obtained after correction for the instrumental broadening) and θ is the angle of diffraction (Haerudin et al., 2010), calculate the average crystal size of silver nanoparticle which equal 25.735nm.

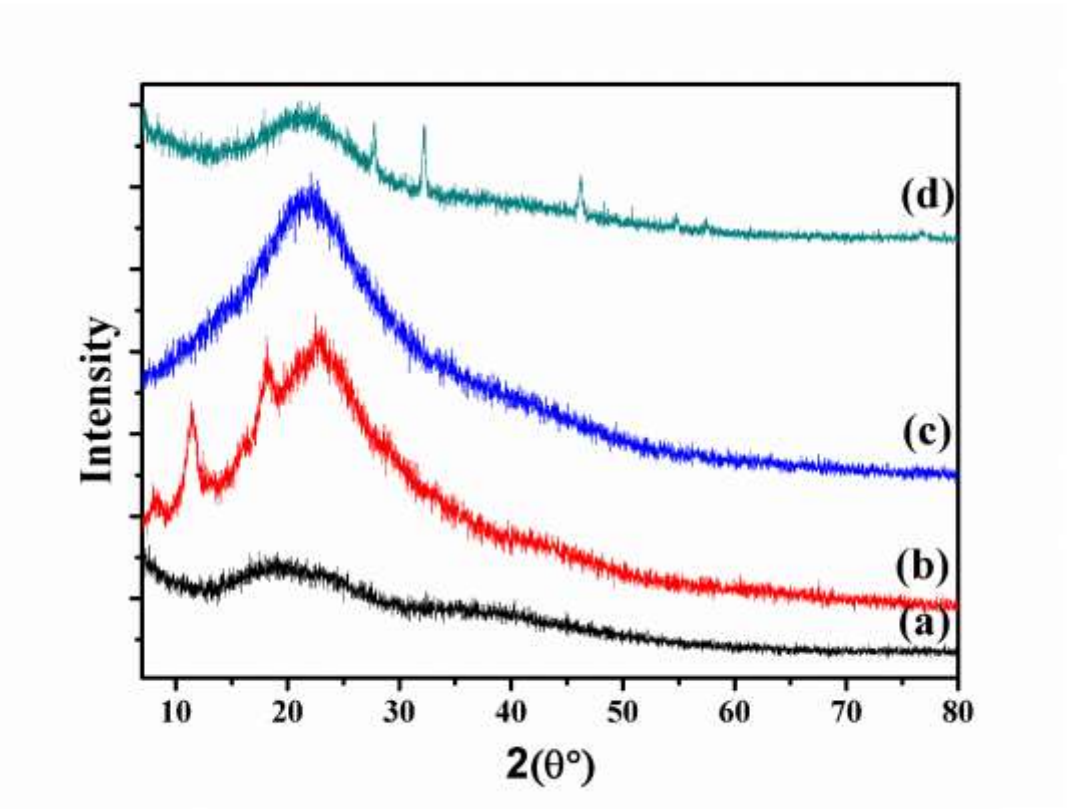

Figure 3 Shows XRD of (a)PPE, (b) Cs, (c) Cs-PPE and (d) Cs-PPE-AgNPs.

As shown in Fig. 4 by using Williamson-Hall plot calculated the strain and the mean grain size of AgNPs by using the following equation

$$\beta \cos\theta = \frac{c\lambda}{t} + 2\varepsilon \sin\theta$$

Found that strain equal 14.5×10^{-3} and grain size 34.6 nm.

In Table 2 we can calculate the lattice strain by this equation at each peak position

$$lattice\ strain = \beta cos\theta / 4sin\theta$$

Table 2 shows the AgNPs crystal size at each peak position

Position of peak (2ɵ)	Crystal size of AgNPS (nm)	Lattice strain
27.78	43.45	0.0033
32.22	31.36	0.0042
46.27	30.58	0.0036
54.77	19.79	0.0036
57.43	20.04	0.0037
76.74	9.19	0.0055

The variation between the calculated values of average crystal size between the Williamson-Hall equation and Scherrer equation is due to the strain correction factor (Joshi et al., 2020).

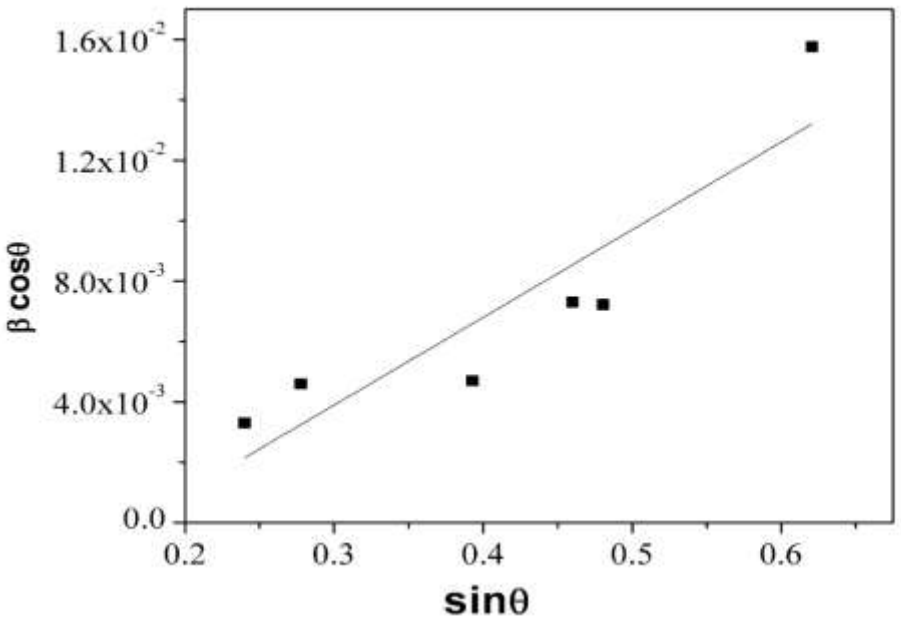

Figure 4 show Williamson-Hall plot for the Cs-PPE-AgNPs..

3.4. Thermal gravimetric analysis (TGA) and differential thermal analysis (DTA).

Thermal gravity (TG) is the branch of thermal analysis which examines the mass change of sample as function of temperature in scanning mode. Differential thermal (DT) is thermal analysis technique used at temperature compare between sample and reference. The thermal decomposition curves provide as the inflection points depict the peak maximum to evaluate the degradation characteristics (Table 3). Simultaneously, percentage mass loss during thermal decomposition investigates (Table 4).

As show in Fig.5 of CS-PPE show that the sample is stable up to 100 °C and above this temperature thermal decomposition occurs in three steps up to 400°C. The thermal decomposition from 100 to 700 °C may be attributed to desorption of bioorganic compounds. For Cs-PPE the first stage at 58.3°C and second stage at 72.92°C of decomposition is happen due to loss of volatile component. The third stage of decomposition from 60.5 to 111.59 °C attributed to sharp endothermic peak at 102 °C crossponding to loss of water and volatile component (Neto et al., 2005; Pereira et al., 2013). The second stage happen between 112 to 400°C attributed to exothermic peak at 150°C for DTA curve and 281°C for TGA with major loss weight 40.33% attributed to decomposition of polymer deacetylation of chitosan.

Add AgNPs to Cs-PPE as show in Fig. 6 lead to shift of first, second and third stages as a result of decreasing water holding capacity. The high of weight loss indicate that the bio-organic material crystallize with AgNPs (Francis et al., 2010). The thermal decomposition of sample contained silver is faster than sample without silver at 800°C the residues mass equal 26.32%.

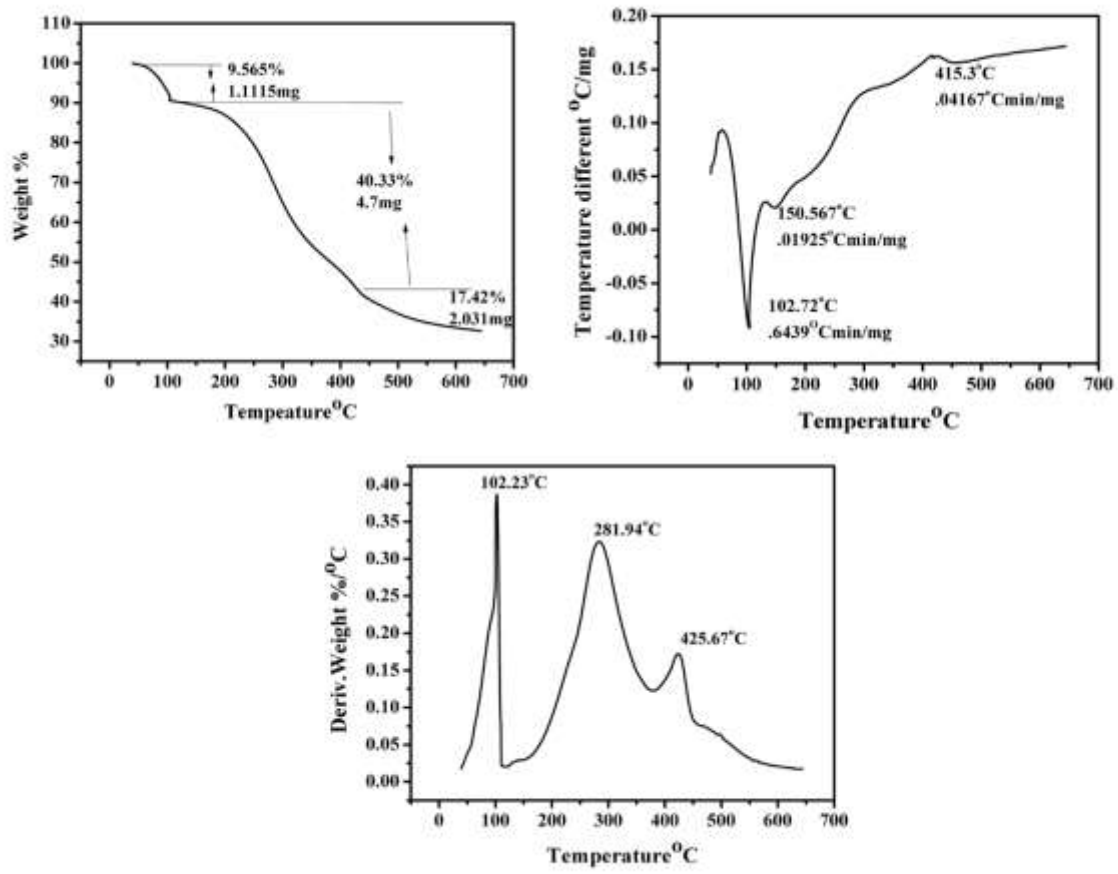

Figure 5 show TGA and DTA of Cs-PPE.

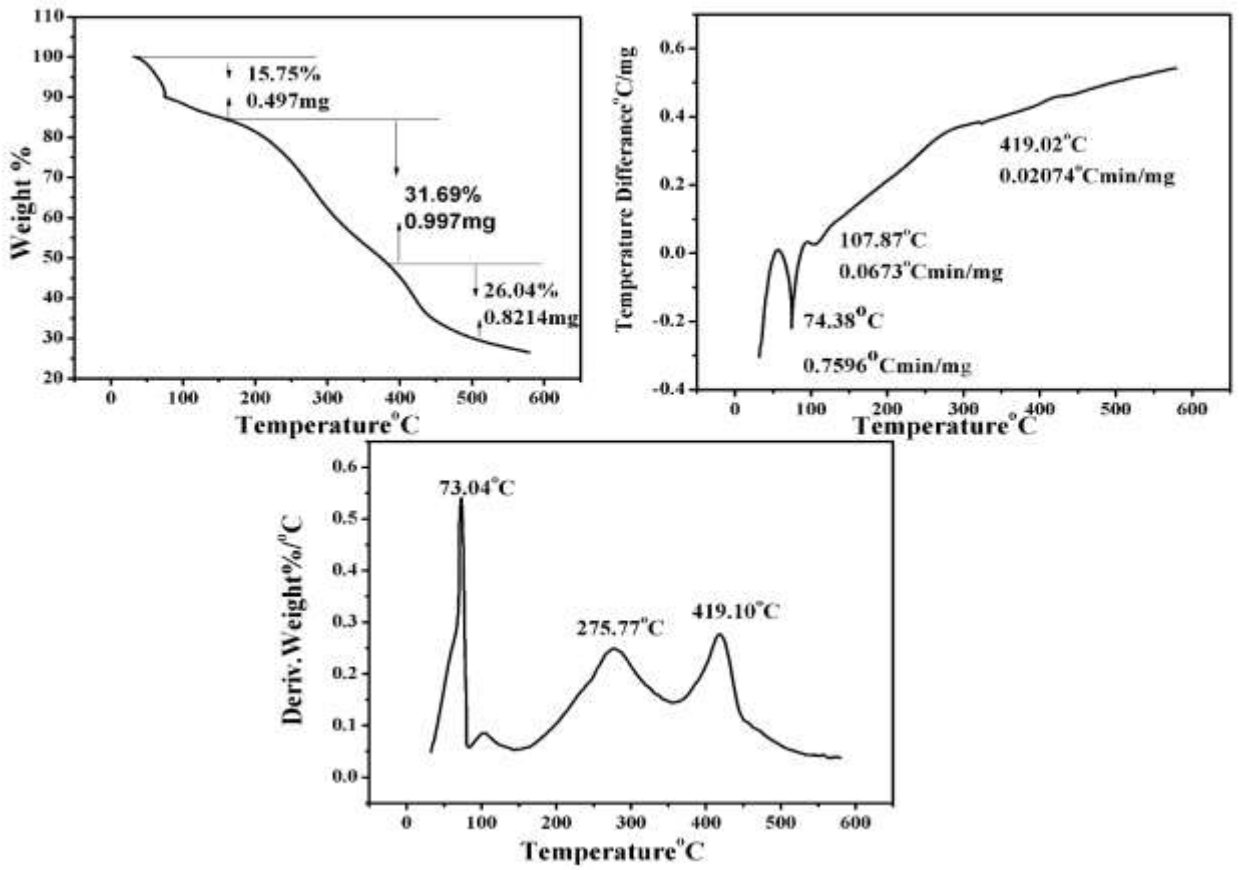

Figure 6 show DTA and TGA of Cs-PPE-AgNPs

Table 3 Thermal decomposition temperature (based on inflection points) of Cs-PEE and Cs-PEE- AgNPs.

Sample	**Inflection point1 ^{0}C**	**Inflection point2 ^{0}C**	**Inflection point3 ^{0}C**
Cs-PPE	102.23	281.94	425.67
Cs-PEE-AgNPs	73.04	275.77	419.10

Table 4

Percentage mass loss and residue of Cs-PEE and Cs-PEE-AgNPs.

Sample	**Mass loss1 %**	**Mass loss2 %**	**Mass loss3 %**	**Final residue %**
Cs-PEE	9.565	40.33	17.42	32.6
Cs-PEE-AgNPs	15.75	31.69	26.04	26.32

3.5. Degradation

Degradation or release of component from the chitosan- pomegranate and silver nanoparticle complex carry by elution technique in aqueous medium technique of different PH values (4, 7and 10), under continuous stirring at 30 ^{0}C.

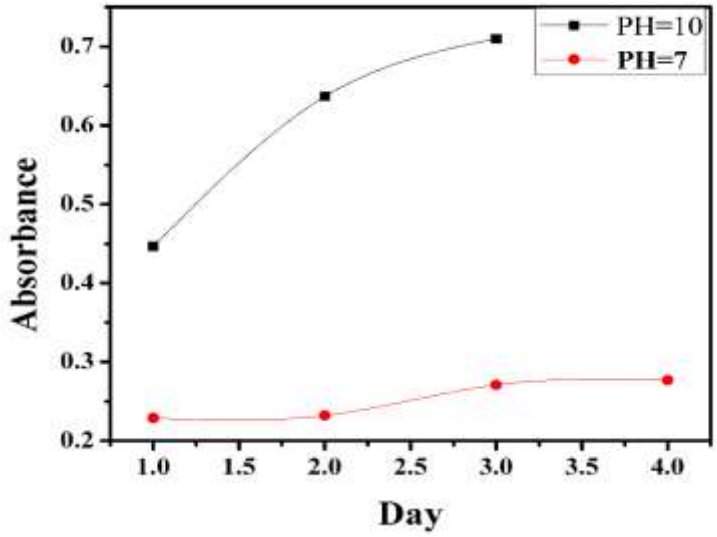

Figure 7(a) show comparison between release of PH 7 and 10 of Cs-PPE-AgNPs.

In acidic medium there's no release happen but release happen at 7 and 10 PH value. From this figure we show that the most release of component happen in first two days and after this two day there's light change happen in strength of peaks and abs increase with increase of PH aqueous solution.

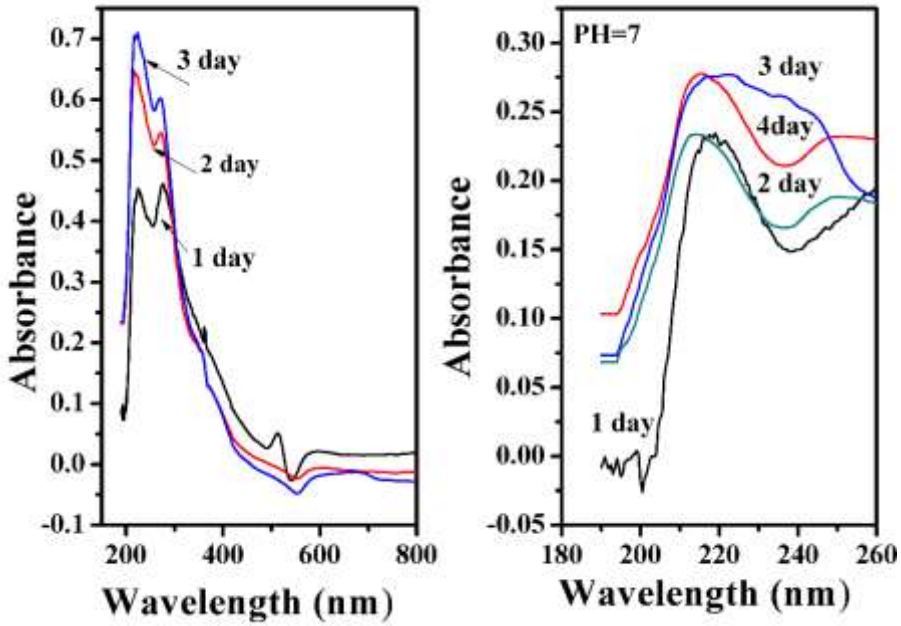

Figure 7(b) show release of sample component in solution at buffer 7 and 10.

3.6 Antibacterial activity

Silver nanoparticles AgNPs have high antibacterial activity. The anti-bacterial activity of different samples demonstrates that both Gram positive and Gram-negative bacteria were inhibited by different solution. The results of the antibacterial activity are depicting in (Table 5). The antibacterial mechanism of solutions may be due to the interaction with lipophilic components of the bacterial membrane, which may cause changes in the permeability of H^+ and K^+, and finally damage the essential functions and cause cell death. In addition, the antibacterial activity against the S.aureus in the solution incorporated with 10 g/L PPE was significantly higher than that incorporated with chitosan or extract alone, suggesting that there is a synergistic action. Adding silver nanoparticle to chitosan and pomegranate peel extract solution by Electrochemical, the ability of chitosan, pomegranate peel extract and silver nanoparticles to inhibit growth greater than chitosan and pomegranate peel extract. In general Gram-positive bacteria consider more sensitive than Gram-negative bacteria to antibacterial compounds (Cao et al., 2010; Kaur et al., 2013).

Table 5 show antibacterial activity expressed as the inhibition zone diameter (mm)

Sample	**E. coli**	**S. Aurous**
Cs	ND	2
PPE	ND	3
Cs - PPE	11	10
Cs -PPE-AgNPs	12.5	17.4

3.7. UV Irradiation

FTIR and UV spectroscopy was used to know change happen due to exposure our solution sample to UV radiation. As shown at UV spectra (Fig. 8) there was decrease in peaks absorption at 259 and 281 nm, disappear of peak at 330 nm and increase of absorption at 405nm after first hour radiation and at FTIR we shown hydrogen peak at 3491 shift to 3451 cm^{-1} , minor broadening of peak at 890 cm^{-1} and decrease of peaks at 1411 and 1155 cm^{-1} suggested that there was good interaction between metal and polymer (Francis et al., 2010; Ismail et al., 2014). All of this suggested that exposed sample to UV irradiation help in enhancement of interaction between chitosan, pomegranate peel extract and silver nanoparticle.

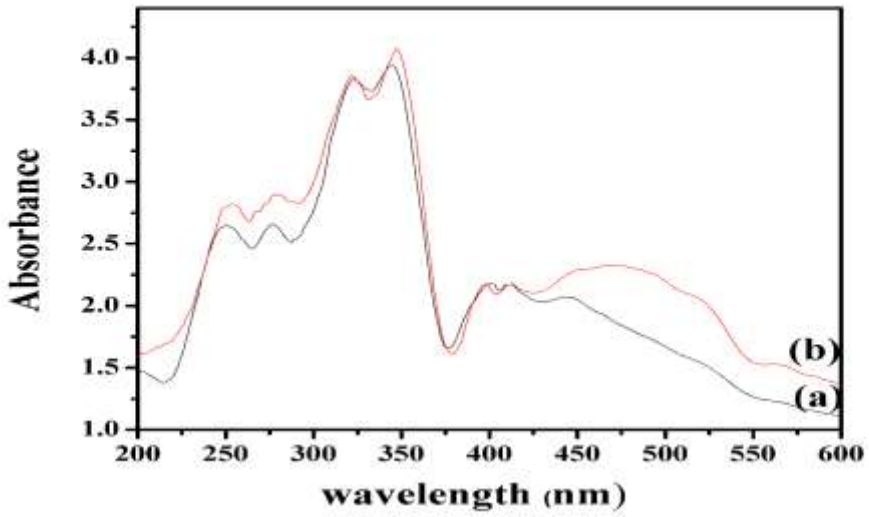

Figure 8 show FTIR of Cs-PPE-AgNPS (a) and after 1h radiation (b).

Table 6 shows the max absorption at 259, 280 and 405nm for four hours radiation of Cs-PPE-AgNPs.

Wave length(nm)	**a**	**b**
259 (aromatic ring)	2.5	2.32
280 (carbonyl group)	2.57	2.1 shift to 295nm
405 (silver nanoparticles)	2.28	2.32

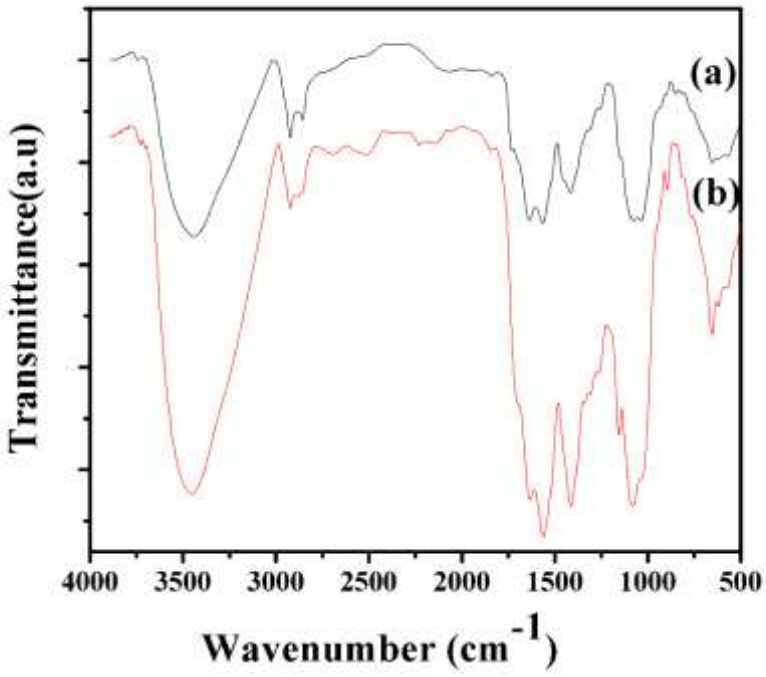

Figure 9 show UV of Cs-PPE-AgNPS (a) and after 1h radiation (b).

3.8. Scanning atomic microscope

Scanning electron microscope picture show that there's across linkage happen between chitosan and pomegranate peel extract which become more homogeneous and denser distributed by adding silver nanoparticles**.**

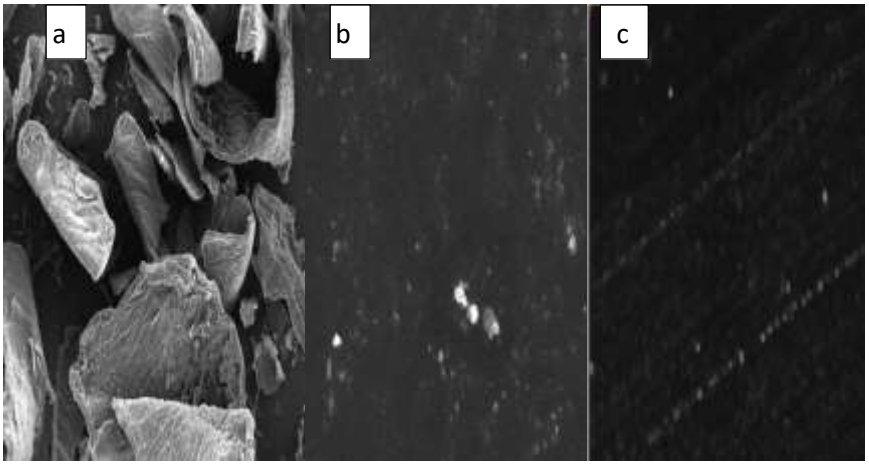

Figure 10 show SEM OF Cs (a), Cs-PPE (b) and Cs-PPE-AgNPs (c).

3.9. TSDC of Chitosan and Pomegranate peel extract.

3.9.1 Effect of polarizing Time.

TSDC spectra of Cs and PPE studied at constant polarizing field 10^6 V/m, constant polarizing temperature 100 ^oC and different polarizing time 15, 20, 30 min (Figs 6 and 7). The quantity of current intensity I_{Max} of peak increase with increasing polarizing time at 15 and 20 min, but at 30 min the saturation happen and the current intensity decrease (Papathanassiou, 1999). Maximum temperature doesn't change with increasing polarizing time which related to glass transition and can be assign as α-relaxation of Cs-PPE.

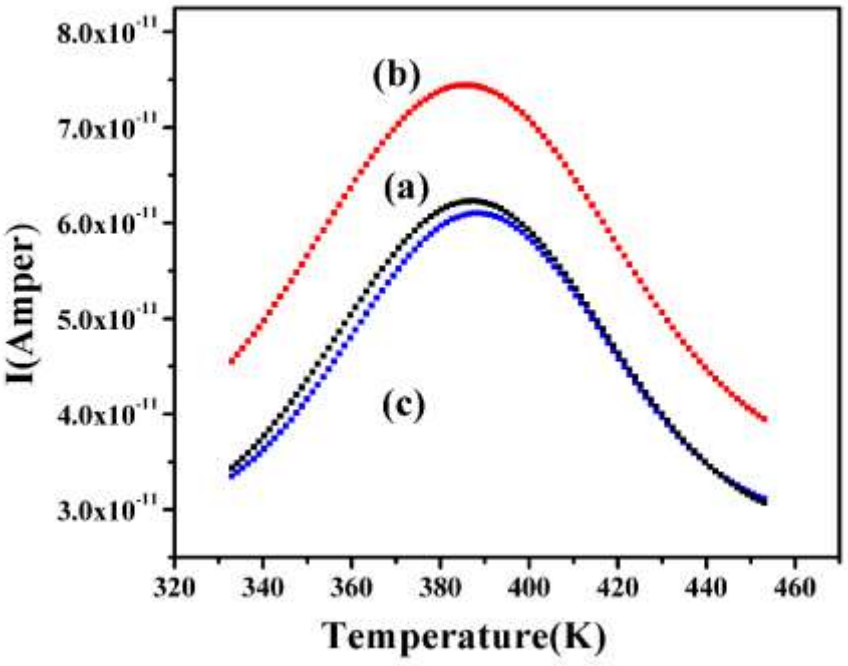

Figure 11 TSDC spectra of (Cs-PPE) (a) t_p=15min, (b) tp=20min and (c) tp=30 min at constant T_p=100^oC and E_P=1×10^6 V/m.

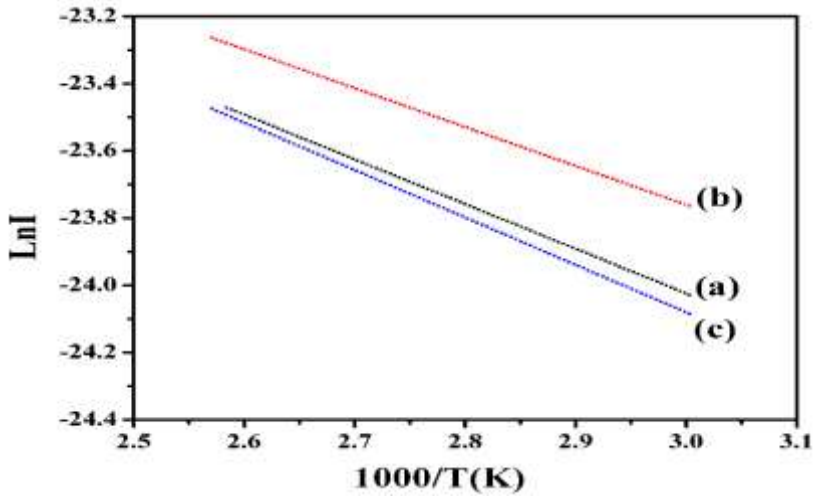

Figure 12 TSDC spectra of (Cs-PPE) describe the relation between Ln (I) versus 1000/T (K^{-1}) of (a) t_p=15min, (b) t_p=20 min and (c) tp=30 min at constant T_p=100°C and E_P=1×10^6 V/m.

Table 6 the molecular parameters of Cs-PPE at different polarizing time.

Boling Time t_P (min)	**Maximum Temperature T_M**	**Maximum Current I_M(10^{-11} Amper)**	**E_a(eV)**
15min	385	6.3	0.206
20min	385	7.44	0.178
30min	386	6.05	0.202

3.9.2. Effect of polarizing Field.

TSDC spectra of Cs with PPE were studied at constant polarizing temperature 373 K polarizing time 15 min with different polarizing field (3, 5, 7 and 10) ×10^5 V/m. As shown in Fig. 13 current intensity increase with increase of polarizing electric field which may be happen due to increase in dipole dipole interaction (Zghal et al., 2014). The activation energy can be calculated from this method as relation between Ln I and 1000/T as depicted in Fig. 14. The high value of activation energy occurs due to cooperative character of molecular motion in glass transition temperature due to strong intra molecular coupling or interaction.

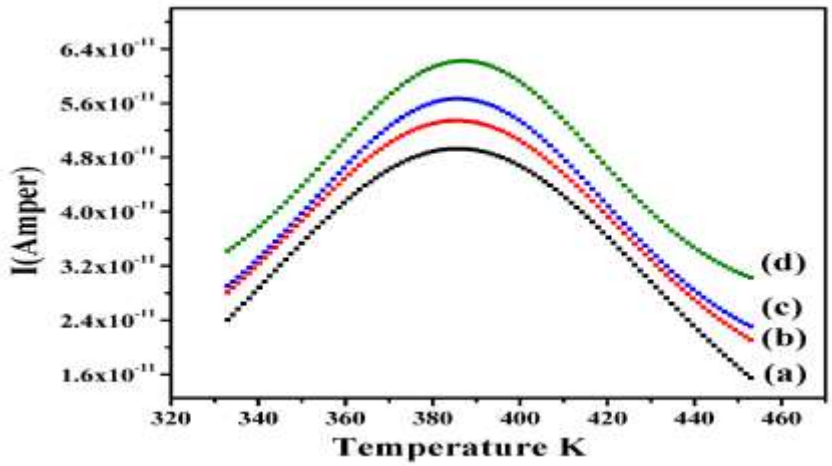

Figure 13 TSDC spectra of (Cs -PPE) (a) E_P =3×10^5, (b) E_P =5×10^5, (c) E_P =7×10^5, (d) E_P=10^6V/m at constant T_p=100°C and t_p=15min.

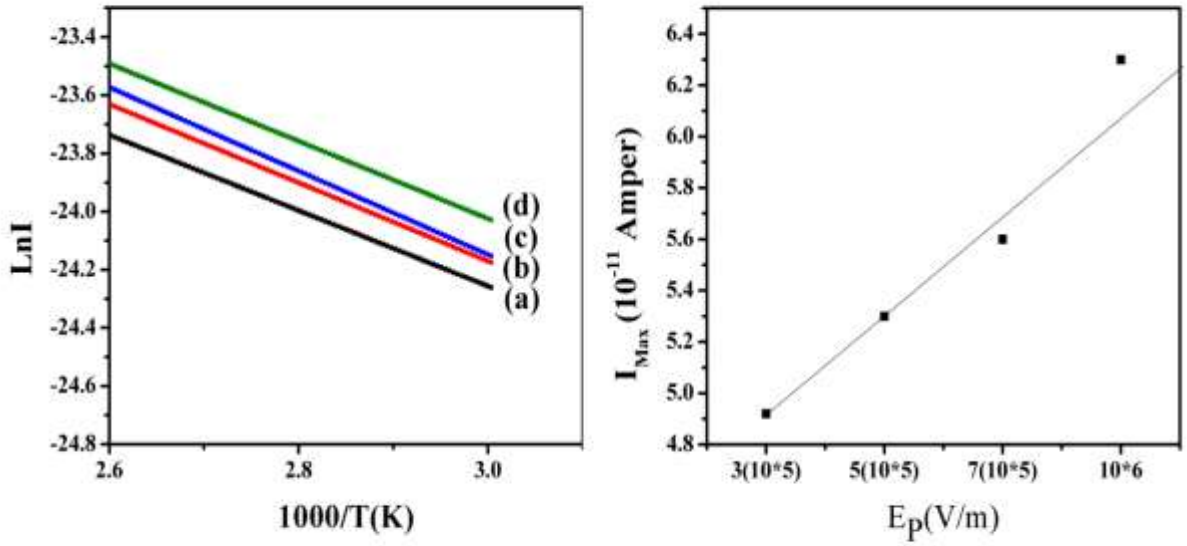

Figure 14 TSDC spectra of (Cs-PPE) describe the relation between Ln(I) versus 1000/T (K^{-1}) of (a) E_P =3×10^5, (b) E_P =5×10^5, (c) E_P=7×10^5 and (d) E_P=10^6V/m at constant T_p=100°C and t_p=15min.

Table 7 the molecular parameters from Arrhenius calculation.

Field E_P (V/m)	**Maximum Temperature T_{max} (K)**	**Maximum Current Imax (10^{-11}A)**	**E_a (eV)**
3(10^5)	386	4.92	0.42
5(10^5)	386	5.3	0.256
7(10^5)	386	5.6	0.254
10^6	386	6.3	0.202

3.9.3 Effect of polarizing temperature.

TSDC spectra of Cs-PPE studied at constant polarizing time 15 min, constant polarizing field 1×10^6 V/m and different polarizing temperature 323, 346, 373 and 428 K (Fig. 15). Increasing polarization temperature, maximum current intensity (I_{Max}) and maximum temperature (T_{Max}) increase and shift to higher position mean that heating lead to change of structure which may change crystallinity degree. In this part T_{Max} > T_P related to space charge contribution.

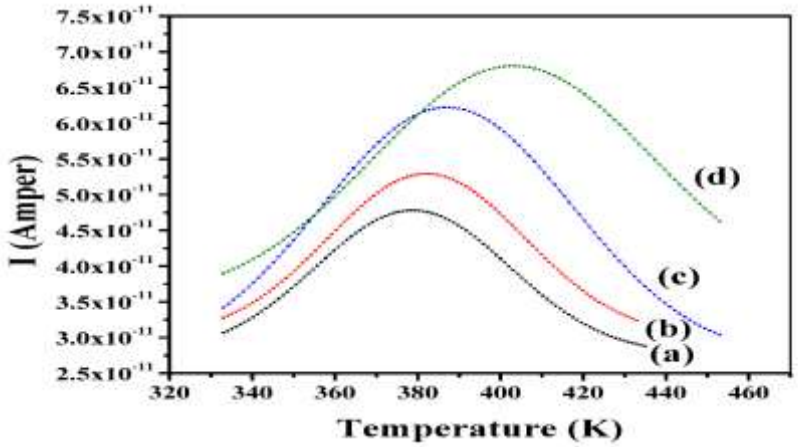

Figure 15 TSDC spectra of (Cs-PPE) (a) T_p=50°C, (b) T_p=75°C, (c) T_p=100°C and (d) Tp=150°C at constant t_p=15min and E_P=1×10^6 V/m.

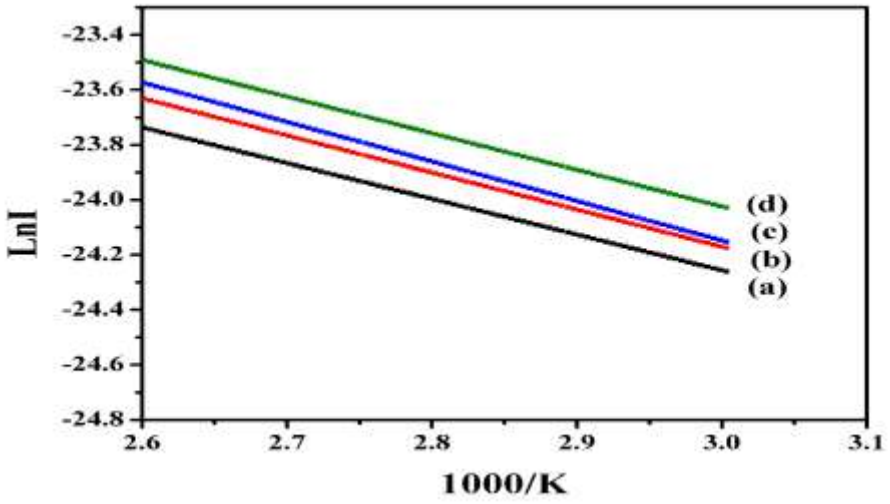

Figure 16 TSDC spectra of (Cs-PPE) describe the relation between Ln(I) versus 1000/T (K^{-1}) of (a) T_p=50°C, (b) T_p=75°C, (c) T_p=100°C and (d) Tp=150°C at constant t_p=15min and E_P=1×10^6 V/m.

Table 8 the molecular parameters of Cs-PPE at different polarizing temperatures.

Boiling Temperature T_p (K)	**Maximum Temperature T_m**	**Maximum current I_m (10^{-11} Amper)**	**E_a (eV)**
323	379	4.7	0.154
348	386	5.27	0.164
373	389	6.3	0.202
423	398	6.83	0.115

3.10 TSDC of Chitosan –Pomegranate peel extracts and silver nanoparticles (Cs-PPE-AgNPs).

3.10.1 Effect of polarizing Field.

TSDC spectra of Cs–PPE-AgNPs were studied at constant polarizing temperature 373K polarizing time 15 min with different polarizing field (3, 5, 7 and 10) $\times 10^5$ V/m.As shown in figure current intensity increase with increase of polarizing electric field which may be happen due to increase in dipole dipole interaction at(5, 7 and 10) $\times 10^5$ V/m (Papathanassiou, 1999). At lower field β peak disappear and by increasing of field the intensity of β and α peak increase. The activation energy can be calculated from this method as relation between Ln I and 1000/T. The high value of activation energy occurs due to cooperative character of molecular motion in glass transition temperature due to strong intra molecular coupling or interaction. The first peak at (316+2) K assigned to β dipolar relaxation associated with orientation of polar side group and the more intense second peak from 362 to 392K was ascribed to α relaxation.

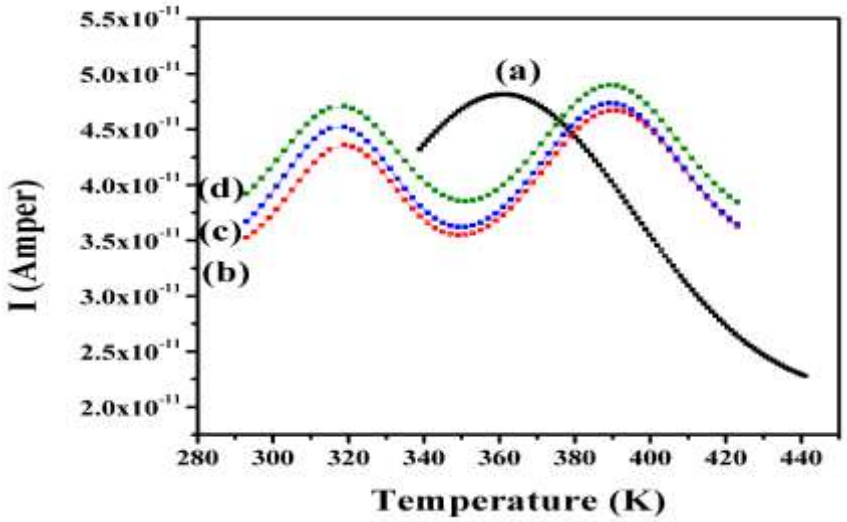

Figure 17 TSDC spectra of (Cs-PPE-AgNPs) (a) $E_P = 3\times10^5$, (b) $E_P=5\times10^5$,(c) $7\times10^5$and (d) $E_P=10^6$V/m at constant T_p=100°C and t_p=15min.

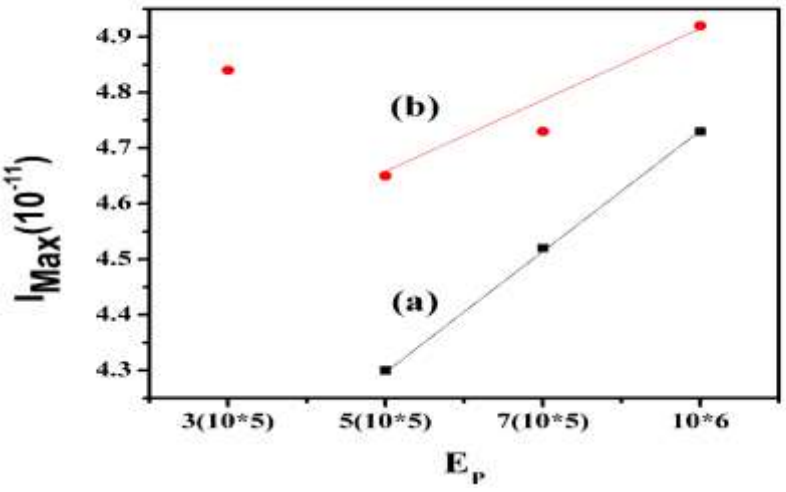

Figure 18 TSDC spectra of (Cs-PPE-AgNPs) describe the relation between I_{Max} versus E_P of (a) first peak and (b) second peak.

Table 9 the molecular parameters of Cs-PPE-AgNPs at different polarizing field.

Field EP (V/m)	**First Maximum Temperature T_{max} (K)**	**First Maximum Current I_{max} (10^{-11}A)**	**E_{a1} (eV)**	**Second Maximum Temperature T_{max} (K)**	**Second Maximum Current I_{max} (10^{-11}A)**	**E_{a2} (eV)**
3×10^5	……	……	…..	362	4.84	0.198
5×10^5	316	4.3	0.301	385	4.65	0.306
7×10^5	316	4.52	0.310	385	4.73	0.292
1×10^6	318	4.7	0.27	392	4.9	0.26

3.10.2 Effect of polarizing temperature.

TSDC spectra of Cs-PPE-AgNPs studied at constant polarizing time 15 min, constant polarizing field 1×10^6 V/m and different polarizing temperature 348, 398, 373 and 423 K. Increasing polarization temperature, maximum current intensity (I_{Max}) and maximum temperature (T_{Max}) increase and shift to higher position (Fig. 19) mean that heating lead to change of structure which may change crystallinity degree. In this part $T_{Max} > T_P$ related to space charge contribution. By increasing temperature β peak become clear and α peak move to higher position. The change in behavior is due to modification of space charge behavior or formation of interface between polymer and AgNPs.

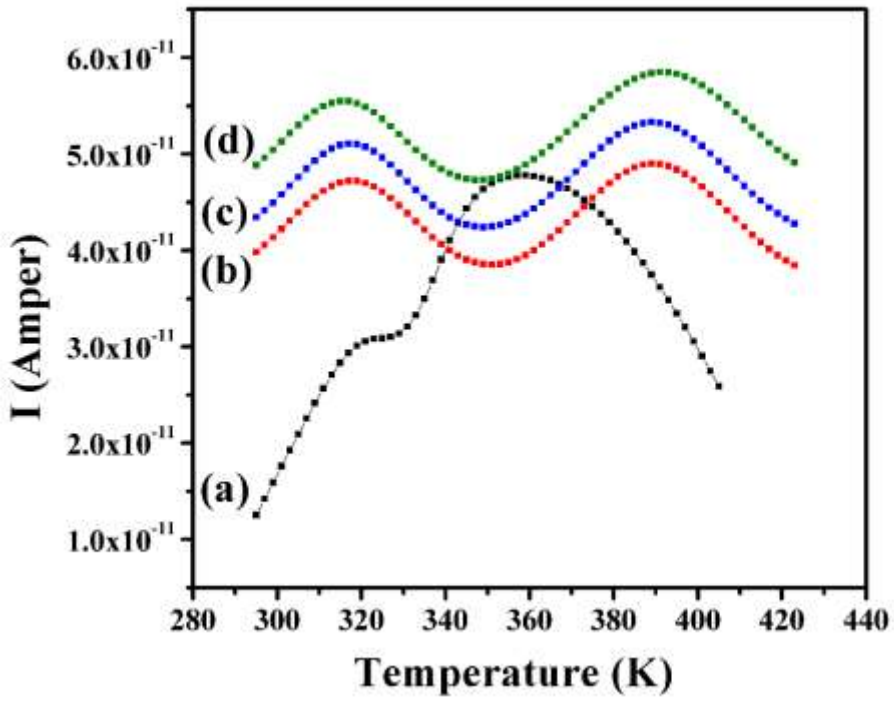

Figure 19 TSDC spectra of (Cs-PPE-AgNPs) (a) T_p=75°C, (b) T_p=100°C, (c) T_p=125°C and (d)) T_p=150°C at constant t_p=15min and $E_P=1\times10^6$ V/m.

Table 10 the molecular parameters of Cs-PPE-AgNPs at different polarizing temperature.

Temperature (°C)	**First Maximum Temperature T_{max} (K)**	**First Maximum Current I_{max} (10^{-11}A)**	**E_{a1} (eV)**	**Second Maximum Temperature T_{max} (K)**	**Second Maximum Current I_{max} (10^{-11}A)**	**E_{a2} (eV)**
348	324	3.04	0.5	358	4.75	0.609
373	318	4.7	0.28	390	4.9	0.29
398	319	5.11	0.29	390	5.32	0.28
423	319	5.59	0.27	392	5.8	0.26

3.10.3 Effect of polarizing Time.

TSDC spectra of Cs-PPE-AgNPs studied at constant polarizing field 10^6V/m, constant polarizing temperature 100°C and different polarizing time 5, 15, 30 min (Fig. 20). At 5 min β peak isn't clear and α peak move to higher position by increase the time.

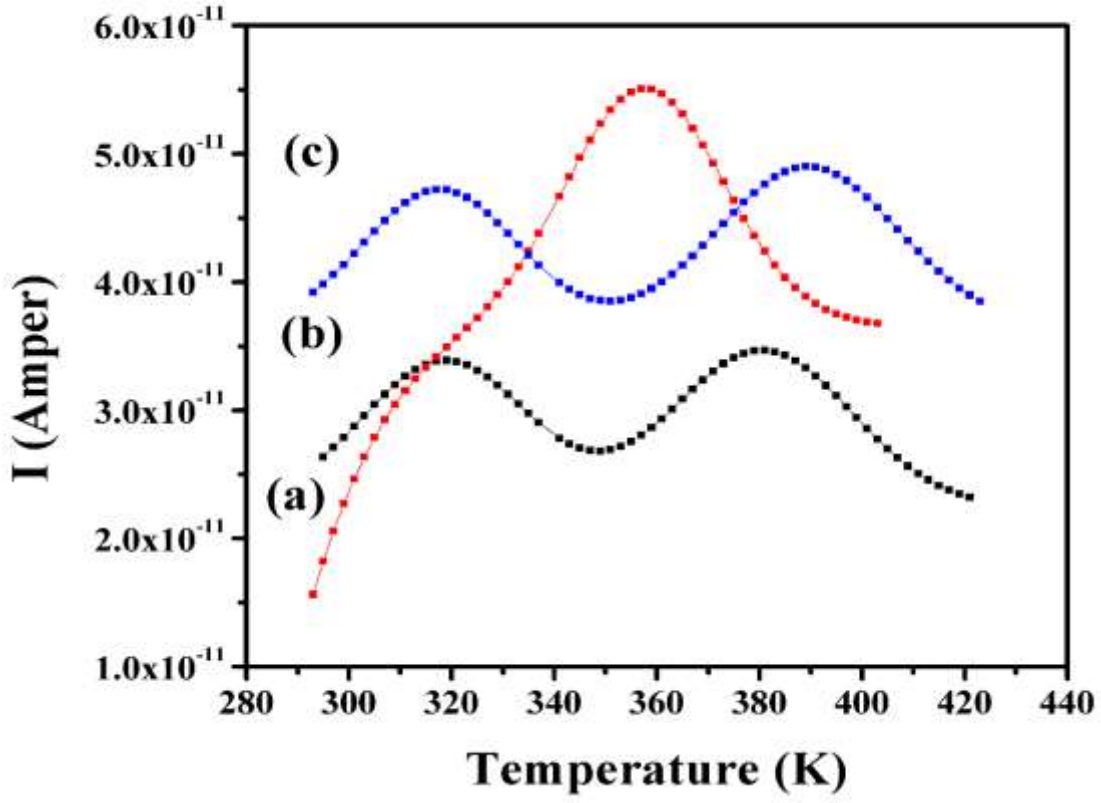

Figure 20 TSDC spectra of (Cs-PPE-AgNPs) (a) t_p=5 min, (b) t_p=15 min and (c) t_p=30 min at constant T_p=100°C and E_P=1×10^6 V/m.

Table 11 the molecular parameters of Cs-PPE-AgNPS at different polarizing time.

Time	First Maximum Temperature T_{max} (K)	First Maximum Current I_{max} (10^{-11}A)	E_{a1} (eV)	Second Maximum Temperature T_{max} (K)	Second Maximum Current I_{max} (10^{-11}A)	E_{a2} (eV)
5 min				357	5.52	0.34
15 min	318	4.7	0.28	390	4.9	0.29
30 min	317	3.25	0.231	382	3.56	0.26

Conclusion

In this work, the Cs-PPE-AgNPs samples have been prepared and investigated via both physical and biological means. Results obtained from FTIR, UV Spectroscopy and XRD measurements prove that there's good interaction between Cs and PPE peel extract and silver nanoparticles. The obtained nanoparticles average size was 34.6 nm. UV Spectroscopy show increase of peak at 405 nm indicates formation of large cluster of AgNPs. Expose Cs-PPE-AgNPs to UV irradiation for 1 h enhance the interaction between the components. Cs-PPE and Cs-PPE-AgNPs also demonstarted a relativity high antibacterial against Escherichia coli and Staphylococcus aureus bacteria. TSDC spectra of Cs-PPE with varying polling time present a single peak at 385 K. The quantity of current intensity I_{Max} of peak increase with increasing polarizing time at 15 and 20 min, but maximum temperature doesn't change with increasing polarizing time which related to glass transition and can be assign as α-relaxation of Cs-PPE. The activation energy calculated and found to be in range of 0.17-0.22 eV. TSDC spectra of Cs-PPE with varying polarizing field present a single peak 368K. This peak refers to alpha relaxation. The current increased linearly with increasing the polling field. The activation energy calculated and found to be in range of 0.202-0.42 eV. TSDC spectra of Cs-PPE with varying polling temperature present a single peak from 379 to 398 K. Increasing polarization temperature, maximum current intensity (I_{Max}) and maximum temperature (T_{Max}) increase and shift to higher position mean that heating lead to change of structure which may change crystallinity degree. In this part $T_{Max} > T_P$ related to space charge contribution. The activation energy calculated and found to be in range of 0.11-0.46 eV. TSDC spectra of Cs-PPE-AgNPs with varying polarizing field present two peaks except $3*10^5$ V/m. The first peak at (316+2) K assigned to β dipolar relaxation associated with orientation of polar side group and the more intense second peak from 362 to 392 K was ascribed to α relaxation. The activation energy calculated and found to be in range of 0.27-0.31 eV for first peak and 0.19-0.33 eV for second peak. TSDC spectra of Cs-PPE-AgNPs with varying polling temperature show change in behavior is due to modification of space charge behavior or formation of interface between polymer and AgNPs. Increasing polarization temperature, maximum current intensity (I_{Max}) and maximum temperature (T_{Max}) increase and shift to higher position mean that heating lead to change of structure which may change crystallinity degree. In this part $T_{Max} > T_P$ related to space charge contribution.

References

Acosta, N., Sánchez, E., Calderón, L., Cordoba-Diaz, M., Cordoba-Diaz, D., Dom, S., & Heras, Á. (2015). Physical stability studies of semi-solid formulations from natural compounds loaded with chitosan microspheres. *Marine drugs, 13*(9), 5901-5919.

Akhtar, S., Ismail, T., Fraternale, D., & Sestili, P. (2015). Pomegranate peel and peel extracts: Chemistry and food features. *Food chemistry, 174*, 417-425.

Bui, V. K. H., Park, D., & Lee, Y.-C. (2017). Chitosan combined with ZnO, TiO2 and Ag nanoparticles for antimicrobial wound healing applications: a mini review of the research trends. *Polymers, 9*(1), 21.

Cao, X., Cheng, C., Ma, Y., & Zhao, C. (2010). Preparation of silver nanoparticles with antimicrobial activities and the researches of their biocompatibilities. *Journal of Materials Science: Materials in Medicine, 21*(10), 2861-2868.

De Leonardis, A., Aretini, A., Alfano, G., Macciola, V., & Ranalli, G. (2008). Isolation of a hydroxytyrosol-rich extract from olive leaves (Olea Europaea L.) and evaluation of its antioxidant properties and bioactivity. *European Food Research and Technology, 226*(4), 653-659.

Fares, R., Bazzi, S., Baydoun, S. E., & Abdel-Massih, R. M. (2011). The antioxidant and anti-proliferative activity of the Lebanese Olea europaea extract. *Plant Foods for Human Nutrition, 66*(1), 58-63.

Francis, L., Balakrishnan, A., Sanosh, K., & Marsano, E. (2010). Hydroxy propyl cellulose capped silver nanoparticles produced by simple dialysis process. *Materials Research Bulletin, 45*(8), 989-992.

Goldsmith, C. D., Vuong, Q. V., Sadeqzadeh, E., Stathopoulos, C. E., Roach, P. D., & Scarlett, C. J. (2015). Phytochemical properties and anti-proliferative activity of Olea europaea L. leaf extracts against pancreatic cancer cells. *Molecules, 20*(7), 12992-13004.

Goldsmith, C. D., Vuong, Q. V., Stathopoulos, C. E., Roach, P. D., & Scarlett, C. J. (2014). Optimization of the aqueous extraction of phenolic compounds from olive leaves. *Antioxidants, 3*(4), 700-712.

Haerudin, H., Pramono, A. W., Kusuma, D. S., Jenie, A., Voelcker, N. H., & Gibson, C. (2010). *Preparation and characterization of chitosan/ontmorillonite MMT nanocomposite systems* University of Indonesia].

Ismail, E. H., Khalil, M. M., Al Seif, F. A., El-Magdoub, F., Bent, A., Rahman, A., & Al, U. (2014). Biosynthesis of gold nanoparticles using extract of grape (Vitis vinifera) leaves and seeds. *Prog Nanotechnol Nanomater, 3*, 1-12.

Joshi, J., Kalainathan, S., Joshi, M., & Parikh, K. (2020). Crystal growth, spectroscopic, second and third order nonlinear optical spectroscopic studies of L-phenylalanine doped ammonium dihydrogen phosphate single crystals. *Arabian Journal of Chemistry*.

Kaur, P., Choudhary, A., & Thakur, R. (2013). Synthesis of chitosan-silver nanocomposites and their antibacterial activity. *Int J Sci Eng Res, 4*(4), 869.

Liu, J., Lu, J.-f., Kan, J., Tang, Y.-q., & Jin, C.-h. (2013). Preparation, characterization and antioxidant activity of phenolic acids grafted carboxymethyl chitosan. *International Journal of Biological Macromolecules, 62*, 85-93.

Loo, Y. Y., Chieng, B. W., Nishibuchi, M., & Radu, S. (2012). Synthesis of silver nanoparticles by using tea leaf extract from Camellia sinensis. *International journal of nanomedicine, 7*, 4263.

López-Mata, M. A., Ruiz-Cruz, S., Silva-Beltrán, N. P., Ornelas-Paz, J. D. J., Zamudio-Flores, P. B., & Burruel-Ibarra, S. E. (2013). Physicochemical, antimicrobial and antioxidant properties of chitosan films incorporated with carvacrol. *Molecules, 18*(11), 13735-13753.

Morsi, M., Oraby, A., Elshahawy, A., & El-Hady, R. A. (2019). Preparation, structural analysis, morphological investigation and electrical properties of gold nanoparticles filled polyvinyl alcohol/carboxymethyl cellulose blend. *Jurnal of Materials Research and Technology, 8*(6), 5996-6010.

Neto, C. d. T., Giacometti, J., Job, A., Ferreira, F., Fonseca, J., & Pereira, M. (2005). Thermal analysis of chitosan based networks. *Carbohydrate polymers, 62*(2), 97-103.

Papathanassiou, A. (1999). Thermal depolarization studies in leukolite (polycrystalline magnesite, MgCO3). *Journal of Physics and Chemistry of Solids, 60*(3), 407-414.

Pereira, F. S., da Silva Agostini, D. L., Job, A. E., & González, E. R. P. (2013). Thermal studies of chitin–chitosan derivatives. *Journal of thermal analysis and calorimetry, 114*(1), 321-327.

Qi, L., Xu, Z., Jiang, X., Hu, C., & Zou, X. (2004). Preparation and antibacterial activity of chitosan nanoparticles. *Carbohydrate research, 339*(16), 2693-2700.

Qin, Y.-Y., Zhang, Z.-H., Li, L., Yuan, M.-L., Fan, J., & Zhao, T.-R. (2015). Physio-mechanical properties of an active chitosan film incorporated with montmorillonite and natural antioxidants extracted from pomegranate rind. *Journal of food science and technology, 52*(3), 1471-1479.

Romainor, A. N. B., Chin, S. F., Pang, S. C., & Bilung, L. M. (2014). Preparation and characterization of chitosan nanoparticles-doped cellulose films with antimicrobial property. *Journal of Nanomaterials, 2014*.

Silverstein, R. M., & Bassler, G. C. (1962). Spectrometric identification of organic compounds. *Journal of Chemical Education, 39*(11), 546.

Suntres, Z. E., Coccimiglio, J., & Alipour, M. (2015). The bioactivity and toxicological actions of carvacrol. *Critical reviews in food science and nutrition, 55*(3), 304-318.

Zghal, E., Namouchi, F., & Guermazi, H. (2014). Study of polarization parameters effect on dipolar relaxation in epoxy-based polymer using thermally stimulated depolarization current. *The European Physical Journal-Applied Physics, 65*(3).

Zhang, J., Xia, W., Liu, P., Cheng, Q., Tahi, T., Gu, W., & Li, B. (2010). Chitosan modification and pharmaceutical/biomedical applications. *Marine drugs, 8*(7), 1962-1987.